# Direct Detection of Light Dark Matter with Magnons

Tanner Trickle,[1,2] Zhengkang Zhang,[1,2] and Kathryn M. Zurek[2,1]

[1] *Department of Physics, University of California, Berkeley, CA 94720*

[2] *Theoretical Physics Group, Lawrence Berkeley National Laboratory, Berkeley, CA 94720*

Scattering of light dark matter with sub-eV energy deposition can be detected with collective excitations in condensed matter systems. When dark matter has spin-independent couplings to atoms or ions, it has been shown to efficiently excite phonons. Here we show that, if dark matter couples to the electron spin, magnon excitations in materials with magnetic dipole order offer a promising detection path. We derive general formulae for single magnon excitation rates from dark matter scattering, and demonstrate as a proof of principle the projected reach of a yttrium iron garnet target for several dark matter models with spin-dependent interactions. This highlights the complementarity of various collective excitations in probing different dark matter interactions.

*Introduction* — Direct detection of dark matter (DM) has undergone a dramatic expansion of scope in recent years. Well-motivated theories where sub-GeV DM arises in a hidden sector/hidden valley, with new weakly or strongly coupled dynamics (see *e.g.* Refs. [1–8] for early examples), have given impetus to new ideas to search for light DM. Conventional nuclear recoils, well-matched kinematically to search for weak-scale DM, are not effective for light DM — once the DM mass drops below the target nucleus mass, the fraction of the DM's kinetic energy that can be deposited on the target falls. Beyond nuclear recoils, better DM-target kinematic matching allows us to probe qualitatively new parameter space, through lighter targets (*e.g.* electrons) with $\sim$eV (as in semiconductors and atoms [9–18] as well as molecules [19, 20]) or $\sim$meV (as in superconductors [21–23] and Dirac materials [24]) energy gaps. Reading out such small energy depositions is achieved through improvements to cryogenic superconducting calorimeters, such as transition edge sensors (TES) and microwave kinetic inductance devices (MKIDs). *Collective* excitations, such as phonons in superfluid helium [25, 26] and crystals [27, 28], open new avenues for good kinematic matching. For example, the presence of $\mathcal{O}$(10-100) meV gapped optical phonons in some systems facilitates the extraction of a large fraction of DM's kinetic energy for DM as light as $\sim$10 keV.

Beyond kinematics, there is also a *dynamics* aspect of the problem — depending on how the DM couples to Standard Model (SM) particles, different target responses are relevant. A familiar example from nuclear recoils is the presence of several nuclear responses – spin-independent (SI), spin-dependent (SD), *etc.* – which can probe different DM-SM interactions [29–32]. Together they provide broad coverage of the DM theory space, with various target nuclei offering complementary information. Another example is dark photon mediated DM: a material with a strong optical response, such as a superconductor, has weak reach since the effective coupling of the dark photon is suppressed due to in-medium effects, while Dirac materials and polar crystals, which have weaker optical response, have excellent reach [24, 27, 28]. Similarly, collective excitations can arise from different degrees of freedom that the DM may couple to, such as charge or spin, and some excitations may be advantageous over others for certain types of DM couplings. Therefore, in order to identify the broadest DM detection strategy, it is important to consider collective excitations of all types.

From this perspective, previous proposals via phonon excitations are aimed at probing SI responses. While they cover many simple DM models, including those with a dark photon or scalar mediator, there are other scenarios that are equally plausible, where the leading DM-SM interactions lead to stronger SD responses. For example, in dark photon mediated models, the DM may in fact be charge neutral, but couples to the dark photon via a higher multipole, *e.g.* magnetic dipole or anapole [30, 32–42]. Also, a spin-0 mediator may dominantly couple to the pseudoscalar current of SM fermions, as opposed to the scalar current. In these scenarios, summarized in Table I, SI responses are suppressed compared to the previously considered cases, and ideas of detecting SD responses are needed.

In this *Letter*, we propose a novel detection path for spin-dependent light DM-electron interactions via magnon excitations. Magnons are quanta of collective spin wave excitations in condensed matter systems that exhibit magnetic dipole order in the ground state. They can be thought of as the SD counterpart of phonons when considering light DM interactions with similar kinematics. We demonstrate as a proof of principle that single magnon excitations can probe interesting DM scenarios, thus broadening the coverage of the DM theory space.

*Magnons in magnetically ordered materials* — Magnetic order can arise in solid state systems due to the interplay between electron-electron interactions, electron kinetic energy and the Pauli exclusion principle (see *e.g.* Refs. [43, 44]). Such systems are usually described by a spin lattice model, such as the Heisenberg model,

$$H = \frac{1}{2}\sum_{l,l'=1}^{N}\sum_{j,j'=1}^{n} J_{ll'jj'}\,\boldsymbol{S}_{lj}\cdot\boldsymbol{S}_{l'j'}\,. \tag{1}$$

| | | | |
|---|---|---|---|
| Magnetic dipole DM | $\mathcal{L} = \frac{g_\chi}{\Lambda_\chi}\bar{\chi}\sigma^{\mu\nu}\chi\, V_{\mu\nu} + g_e\bar{e}\gamma^\mu e\, V_\mu$ | $\hat{\mathcal{O}}^\alpha_\chi = \frac{4g_\chi g_e}{\Lambda_\chi m_e}\left(\delta^{\alpha\beta} - \frac{q^\alpha q^\beta}{q^2}\right)\hat{S}^\beta_\chi$ | $\bar{\sigma}_e = \frac{g_\chi^2 g_e^2}{\pi}\frac{6m_\chi^2+m_e^2}{\Lambda_\chi^2(m_\chi+m_e)^2}$ |
| Anapole DM | $\mathcal{L} = \frac{g_\chi}{\Lambda_\chi^2}\bar{\chi}\gamma^\mu\gamma^5\chi\,\partial^\nu V_{\mu\nu} + g_e\bar{e}\gamma^\mu e\, V_\mu$ | $\hat{\mathcal{O}}^\alpha_\chi = \frac{2g_\chi g_e}{\Lambda_\chi^2 m_e}\epsilon^{\alpha\beta\gamma} iq^\beta \hat{S}^\gamma_\chi$ | $\bar{\sigma}_e = \frac{g_\chi^2 g_e^2}{\pi}\frac{3\alpha^2\mu_{\chi e}^2}{2\Lambda_\chi^4}$ |
| Pseudo-mediated DM | $\mathcal{L} = g_\chi\bar{\chi}\chi\phi + g_e\bar{e}\, i\gamma^5 e\,\phi$ | $\hat{\mathcal{O}}^\alpha_\chi = -\frac{g_\chi g_e}{q^2 m_e} iq^\alpha \mathbb{1}_\chi$ | $\bar{\sigma}_e = \frac{g_\chi^2 g_e^2}{4\pi}\frac{\mu_{\chi e}^2}{\alpha^2 m_e^4}$ |

TABLE I. Dark matter models with SD interactions considered in this work. $\chi$ is a spin-1/2 DM particle, and $V$, $\phi$ are ultralight (typically $\ll$ eV) spin-1, spin-0 mediators, respectively. $\hat{\mathcal{O}}^\alpha_\chi$ (with $\alpha = 1, 2, 3$ denoting the Cartesian coordinates) is the nonrelativistic operator that couples to the electron spin, as defined in Eq. (4). $q \equiv |\boldsymbol{q}|$ is the momentum transfer, and $\hat{S}^\alpha_\chi = \sigma^\alpha/2$ is the DM spin operator. $\bar{\sigma}_e$ is the reference cross section defined in Eq. (11) that we will use to present the reach.

Here $l, l'$ label the magnetic unit cells, and $j, j'$ label the magnetic atoms/ions inside the unit cell. Depending on the sign of the exchange coupling $J_{ll'jj'}$, the spins $\boldsymbol{S}_{lj}$ and $\boldsymbol{S}_{l'j'}$ tend to align or anti-align. The low energy excitations are obtained by applying the Holstein-Primakoff transformation to expand the spins around the ordered ground state in terms of bosonic creation and annihilation operators $\hat{a}^\dagger, \hat{a}$. The quadratic part of the Hamiltonian can then be diagonalized via a Bogoliubov transformation (see Appendix for details),

$$\begin{pmatrix} \hat{a}_{j,\boldsymbol{k}} \\ \hat{a}^\dagger_{j,-\boldsymbol{k}} \end{pmatrix} = \begin{pmatrix} \mathrm{U}_{j\nu,\boldsymbol{k}} & \mathrm{V}_{j\nu,\boldsymbol{k}} \\ \mathrm{V}^*_{j\nu,-\boldsymbol{k}} & \mathrm{U}^*_{j\nu,-\boldsymbol{k}} \end{pmatrix} \begin{pmatrix} \hat{b}_{\nu,\boldsymbol{k}} \\ \hat{b}^\dagger_{\nu,-\boldsymbol{k}} \end{pmatrix}, \tag{2}$$

$$H = \sum_{\nu=1}^{n}\sum_{\boldsymbol{k}\in 1\mathrm{BZ}} \omega_{\nu,\boldsymbol{k}}\hat{b}^\dagger_{\nu,\boldsymbol{k}}\hat{b}_{\nu,\boldsymbol{k}}\,, \tag{3}$$

so that $\hat{b}^\dagger, \hat{b}$ are creation and annihilation operators of the canonical magnon modes, which are collective excitations of the spins. For a system with $N$ magnetic unit cells and $n$ magnetic atoms/ions in the unit cell, there are $n$ magnon branches, labeled by $\nu$, with $N$ modes on each branch, labeled by momentum vectors $\boldsymbol{k}$ within the first (magnetic) Brillouin zone (1BZ). The $n \times n$ matrices U, V can be calculated for each $\boldsymbol{k}$.

*Magnon excitation from dark matter scattering* — If the DM couples to the electron spin,[1] it can scatter off the target material and create magnon excitations. Suppose the nonrelativistic effective Lagrangian takes the form

$$\mathcal{L} = -\sum_{\alpha=1}^{3}\hat{\mathcal{O}}^\alpha_\chi(\boldsymbol{q})\hat{S}^\alpha_e, \tag{4}$$

where $\alpha$ denotes the Cartesian coordinates, and $\boldsymbol{q}$ is the momentum transfer from the DM to the target. The operators $\hat{\mathcal{O}}_\chi$ for the three DM models we consider are listed in Table I. Focusing on transitions from the ground state to single magnon states $|\nu, \boldsymbol{k}\rangle$, we obtain the matrix element as (see Appendix for details)

$$\mathcal{M}^{s_i s_f}_{\nu,\boldsymbol{k}}(\boldsymbol{q}) = \delta_{\boldsymbol{q},\boldsymbol{k}+\boldsymbol{G}}\frac{1}{\sqrt{N\Omega}}\sum_{\alpha=1}^{3}\langle s_f|\hat{\mathcal{O}}^\alpha_\chi(\boldsymbol{q})|s_i\rangle\,\epsilon^\alpha_{\nu,\boldsymbol{k},\boldsymbol{G}}\,, \tag{5}$$

where $\Omega$ is the volume of the magnetic unit cell, $\boldsymbol{G}$ denotes a reciprocal lattice vector, and $|s_{i,f}\rangle$ are the initial and final DM spin states. $\boldsymbol{\epsilon}_{\nu,\boldsymbol{k},\boldsymbol{G}}$ is the analog of polarization vectors for the magnon modes,

$$\boldsymbol{\epsilon}_{\nu,\boldsymbol{k},\boldsymbol{G}} = \sum_{j=1}^{n}\sqrt{\frac{S_j}{2}}\left(\mathrm{V}_{j\nu,-\boldsymbol{k}}\boldsymbol{r}^*_j + \mathrm{U}^*_{j\nu,\boldsymbol{k}}\boldsymbol{r}_j\right)e^{i\boldsymbol{G}\cdot\boldsymbol{x}_j}\,, \tag{6}$$

where $r^\alpha_j \equiv R^{\alpha 1}_j + iR^{\alpha 2}_j$ parameterize the spin orientations in the ground state,

$$S^\alpha_{lj} = \sum_\beta R^{\alpha\beta}_j S'^\beta_{lj}\,, \quad \{\langle S'^1_{lj}\rangle, \langle S'^2_{lj}\rangle, \langle S'^3_{lj}\rangle\} = \{0, 0, S_j\}\,, \tag{7}$$

and $\boldsymbol{x}_j \equiv \boldsymbol{x}_{lj} - \boldsymbol{x}_l$ is the position of the $j$th site within a magnetic unit cell. As a simple example, a ferromagnet with one magnetic ion per unit cell ($n = 1$) has $\boldsymbol{r} = (1, i, 0)$, $U = 1$, $V = 0$, and thus, $\boldsymbol{\epsilon} = \sqrt{S/2}\,(1, i, 0)$ for all $\boldsymbol{k}$ and $\boldsymbol{G}$, reminiscent of a photon polarization vector.

From Eq. (5) we see that for any given $\boldsymbol{q}$, only the magnon modes with a definite momentum $\boldsymbol{k}$ within the 1BZ that satisfies $\boldsymbol{q} = \boldsymbol{k} + \boldsymbol{G}$, for some $\boldsymbol{G}$, can be excited, as a consequence of lattice momentum conservation. Summing over $s_f$ and averaging over $s_i$, we obtain

$$\overline{|\mathcal{M}_{\nu,\boldsymbol{k}}(\boldsymbol{q})|^2} = \frac{\delta_{\boldsymbol{q},\boldsymbol{k}+\boldsymbol{G}}}{N\Omega^2}\,\mathrm{tr}\left(\hat{\rho}_\chi\hat{\mathcal{O}}^\alpha_\chi(\boldsymbol{q})\hat{\mathcal{O}}^{\dagger\beta}_\chi(\boldsymbol{q})\right)\epsilon^\alpha_{\nu,\boldsymbol{k},\boldsymbol{G}}\epsilon^{*\beta}_{\nu,\boldsymbol{k},\boldsymbol{G}}\,, \tag{8}$$

where $\hat{\rho}_\chi = \frac{1}{2S_\chi+1}\mathbb{1}_{2S_\chi+1}$ is the density matrix for the spin of the incoming DM. The total event rate per unit target mass $R$ is then obtained as

$$R = \frac{1}{\rho_T}\frac{\rho_\chi}{m_\chi}\int d^3v_\chi\, f(\boldsymbol{v}_\chi)\sum_\nu\sum_{\boldsymbol{k}\in 1\mathrm{BZ}}\Gamma_{\nu,\boldsymbol{k}}(\boldsymbol{v}_\chi)\,, \tag{9}$$

$$\Gamma_{\nu,\boldsymbol{k}}(\boldsymbol{v}_\chi) = 2\pi\sum_{\boldsymbol{q}=\boldsymbol{k}+\boldsymbol{G}}\overline{|\mathcal{M}_{\nu,\boldsymbol{k}}(\boldsymbol{q})|^2}\,\delta\left(E_{\chi_i} - E_{\chi_f} - \omega_{\nu,\boldsymbol{k}}\right)\,, \tag{10}$$

[1] The spins in the lattice model may also contain orbital angular momentum components. In that case, deriving the DM-lattice spin coupling requires a careful matching calculation, which we leave for future work. Here we assume negligible orbital angular momentum, noting that this is the case for many familiar materials where 3d electrons are responsible for the magnetic order.

where $\rho_T$ is the target mass density, $\rho_\chi = 0.3\,\mathrm{GeV/cm^3}$ is the local DM energy density, $E_{\chi_i} = \frac{1}{2}m_\chi v_\chi^2$, $E_{\chi_f} = (m_\chi \boldsymbol{v}_\chi - \boldsymbol{q})^2/(2m_\chi)$. We assume the DM velocity distribution $f(\boldsymbol{v}_\chi)$ is Maxwell-Boltzmann, with dispersion 220 km/s, truncated by the galactic escape velocity 500 km/s, and boosted to the target rest frame by the Earth's velocity in the galactic rest frame, 240 km/s. We take the continuum limit of the magnon momentum sum via $\sum_{\boldsymbol{k}\in 1\mathrm{BZ}} \to N\Omega \int \frac{d^3k}{(2\pi)^3}$, which makes it apparent that factors of $N$ cancel out in the final result for $R$.

*Projected reach* — As a first demonstration of the DM detection concept, we consider a yttrium iron garnet (YIG, $Y_3Fe_5O_{12}$) target. YIG is a classic ferrimagnetic material that has been extensively studied and well-characterized, and can be readily synthesized with high quality [45, 46]. It has been exploited for axion DM detection via absorption in an external magnetic field, read out in a cavity [47–49]. Here we focus on DM scattering for which external fields are not necessary for producing a signal, so we envision zero-field readout. Particular detection schemes will be explored in future work.

YIG has 20 magnetic ions $Fe^{3+}$ in the magnetic unit cell (which coincides with the crystal primitive cell), and thus 20 magnon branches. The effective spin on each lattice site is $S_j = 5/2$ ($j = 1, \ldots, 20$), which comes from the five 3d electrons of $Fe^{3+}$ with quenched orbital angular momentum. The ground state is ferrimagnetic, with the 12 tetrahedral-site and 8 octahedral-site spins pointing in opposite directions. Taking the crystal parameters from Ref. [50] and Heisenberg model parameters from Ref. [45], we diagonalize the magnon Hamiltonian using the algorithm of Ref. [51] to obtain the magnon spectrum $\omega_{\nu,\boldsymbol{k}}$ (see Fig. 2 in Appendix) and the U, V matrices that enter the rate formulae. For simplicity, we fix the direction of the DM wind to be parallel (perpendicular) to the ground state spins for the magnetic dipole and anapole (pseudo-mediated) models, which maximizes the event rate. For fixed target orientation, we find a daily modulation of $\mathcal{O}(10\%)$, which could be utilized for distinguishing DM signals from backgrounds. Following common practice, we present the projected reach in terms of a reference cross section $\bar{\sigma}_e$ defined from DM-free electron scattering. Here we generalize the definition in Ref. [9] beyond SI interactions by defining

$$\bar{\sigma}_e \equiv \frac{\mu_{\chi e}^2}{16\pi m_\chi^2 m_e^2} \overline{|\mathcal{M}_{\mathrm{free}}|^2}\,(q = \alpha m_e, v^\perp = \alpha)\,, \qquad (11)$$

where $\mu_{\chi e}$ is the DM-electron reduced mass, $\alpha = 1/137$ is the fine structure constant, and $v^\perp$ is the component of the relative velocity perpendicular to $\boldsymbol{q}$. The reference cross-section for each model is given in Table I.

Our results are shown in Fig. 1 for $m_\chi$ up to 10 MeV, assuming 3 events on a YIG target (colored solid curves) with kilogram-year exposure and, following convention for easy comparison to other experiments, no background.[2] Beyond 10 MeV, the DM's de Broglie wavelength becomes comparable to the size of $Fe^{3+}$, invalidating the simple Heisenberg model description; however, electron excitations are expected to have sensitivity in this mass regime [9–14, 17, 18] (though the precise results are not currently available for the SD models considered here). We consider several detector thresholds $\omega_{\mathrm{min}}$ corresponding to capabilities of TESs expected within the next few years (40 meV) and further into the future (10 meV, 1 meV). Also shown in the plots are contours of model parameters in the magnon sensitivity region (gray). For the pseudo-mediated DM model, the mediator-electron coupling is severely constrained by white dwarf cooling to be $g_e \lesssim 2 \times 10^{-13}$, so that $g_\chi$ has to be $\mathcal{O}(1)$ to produce a detectable signal. We thus consider the case where $\chi$ constitutes a 5% subcomponent of DM to evade self-interacting dark matter (SIDM) constraints, and show contours of $g_\chi$ with $g_e$ saturating its upper bound. For the magnetic dipole and anapole DM models, on the other hand, stellar and cosmological constraints on $g_e$ decouple in the $m_V \to 0$ limit, assuming the dark photon $V$ couples to SM particles only via kinetic mixing with the photon. Meanwhile, we have checked that SIDM constraints on $g_\chi$ are satisfied in the parameter space shown.[3]

To gain some analytical intuition, we note that for momentum transfer well within the 1BZ, corresponding to $m_\chi \lesssim 0.1$ MeV for a YIG target, the magnon excitation rate can be estimated via an effective $n = 1$ ferromagnetic model. This is because in the $q \to 0$ limit, the external probe $\hat{\mathcal{O}}_\chi^\alpha$ acts like a uniform magnetic field. In a semiclassical picture, this causes all the spins in the target to precess in phase, so the angle between them, and thus the total energy of the Heisenberg model, stays the same. As a result, only the *gapless* mode(s), *i.e.* Goldstone mode(s) of the broken rotational symmetry, can be excited (we have checked this explicitly for YIG). Even for finite $q$, gapped magnon contributions are suppressed by powers of $aq$, where $a$ is the lattice spacing, and thus subdominant for $q \ll a^{-1}$ ($\simeq 0.2$ keV for YIG). For a

[2] For calorimetric readout, the backgrounds are expected to be similar to other experiments reading out meV-eV energy depositions: radiogenic backgrounds are not expected to be problematic at such low energies, while coherent scattering from high-energy photons can be suppressed with an active veto, leaving *pp* solar neutrinos the main irreducible background. We expect the latter to be at most a few events per kilogram-year, as estimated from neutrino-nucleus scattering (see *e.g.* Refs. [22, 52]).

[3] Additional constraints on these models may arise from production of $\chi$ in supernova (SN) and in the early universe, which are however dependent on $\Lambda_\chi$ and the ultraviolet (UV) completion above that scale. For example, if $\Lambda_\chi \sim m_\chi$ and the UV completion involves millicharged particles [53, 54] with couplings $\sim g_\chi$, both SN and $N_{\mathrm{eff}}$ bounds can be evaded with $g_\chi g_e \lesssim 10^{-10}$ for the magnetic dipole DM model; for the anapole DM model, the magnon sensitivity region correspond to the SN trapping regime, and further model building is needed to evade $N_{\mathrm{eff}}$ constraints.

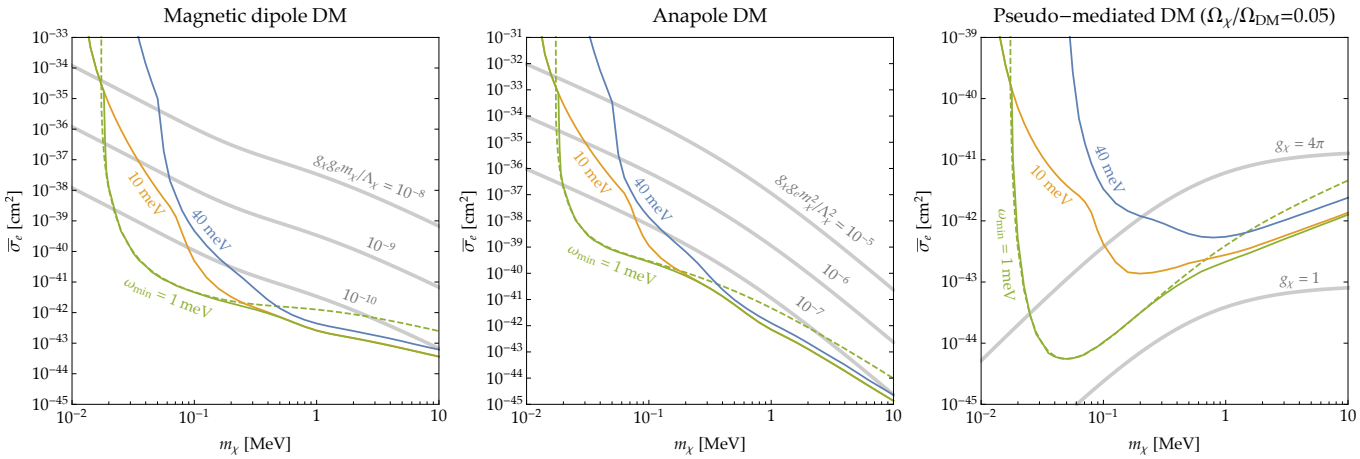


FIG. 1. Projected reach for the DM models in Table I for a YIG target, assuming three events with kilogram-year exposure, for several magnon detection thresholds $\omega_{\rm min}$ (solid). Also shown are the results of a Heisenberg ferromagnet with the same mass and spin densities as YIG, and the same magnon dispersion as the low-energy gapless modes of YIG, for $\omega_{\rm min} = 1\,\text{meV}$ (dashed); they coincide with the YIG curves for $0.02\,\text{MeV} \lesssim m_\chi \lesssim 0.1\,\text{MeV}$, which can be understood from the effective theory argument in the text. The gray contours show the model parameters in the magnon sensitivity regions. For the pseudo-mediated model, we consider a DM subcomponent to evade SIDM constraints, and let $g_e$ saturate the white dwarf cooling bound.

ferrimagnet, like YIG, we can integrate out the gapped modes to arrive at an effective theory, where the unit cell has been coarse-grained and the only relevant degree of freedom is the total spin density $n_s$. There is only one magnon branch in this effective $n = 1$ ferromagnetic theory, which matches the gapless branch of the original ferrimagnet for $k \ll a^{-1}$. For YIG, the total spin density is $S_{\rm cell} = (12-8)\times 5/2 = 10$ per unit cell volume $\Omega = a^3/2$, with $a \simeq 12.56\,\text{Å}$, *i.e.* $n_s = 20/a^3 \simeq (4.6\,\text{Å})^{-3}$. The effective exchange coupling can be shown to be $J_{\rm eff} \simeq -4\,\text{K} = -0.35\,\text{meV}$ [45], resulting in a quadratic magnon dispersion $\omega = |J_{\rm eff}|S_{\rm cell}\,(ak)^2 \simeq k^2/(7\,\text{MeV})$ at small $k$. For this $n = 1$ ferromagnetic theory, we obtain the following approximate analytical result for the DM scattering rate (see Appendix for details),

$$
\begin{aligned}
R &\simeq \frac{n_s}{\rho_T}\frac{\rho_\chi}{m_\chi}\int d^3v_\chi\, f(\boldsymbol{v}_\chi)\cdot \\
&\qquad \int \frac{d^3q}{8\pi^2}\,\text{tr}\big(\hat{\rho}_\chi \hat{\mathcal{O}}_\chi^+(\boldsymbol{q})\hat{\mathcal{O}}_\chi^{\dagger-}(\boldsymbol{q})\big)\,\delta\left(E_{\chi_i} - E_{\chi_f} - \omega\right)\,, \\
&\simeq 3\,(\text{kg}\cdot\text{yr})^{-1}\left(\frac{n_s}{(4.6\,\text{Å})^{-3}}\right)\left(\frac{4.95\,\text{g/cm}^3}{\rho_T}\right)\left(\frac{0.1\,\text{MeV}}{m_\chi}\right) \\
&\qquad \int d^3v_\chi\, f(\boldsymbol{v}_\chi)\left(\frac{10^{-3}}{v_\chi}\right)\left(\frac{\hat{R}}{4\times 10^{-27}}\right), \qquad (12)
\end{aligned}
$$

where $\hat{\mathcal{O}}_\chi^\pm \equiv \hat{\mathcal{O}}_\chi^1 \pm i\hat{\mathcal{O}}_\chi^2$, and

$$
\begin{aligned}
\hat{R} &= m_e^2\int\frac{d^3q}{2\pi q}\,\text{tr}\big(\hat{\rho}_\chi\hat{\mathcal{O}}_\chi^+\hat{\mathcal{O}}_\chi^{\dagger-}\big)\,\delta\left(\cos\theta - \frac{q}{2m_\chi v_\chi} - \frac{\omega}{v_\chi q}\right) \\
&= \begin{cases} \frac{2g_\chi^2 g_e^2(1+\langle c^2\rangle)}{\Lambda_\chi^2}(q_{\rm max}^2 - q_{\rm min}^2) & \text{(magnetic dipole)}\,, \\ \frac{g_\chi^2 g_e^2(1+\langle c^2\rangle)}{4\Lambda_\chi^4}(q_{\rm max}^4 - q_{\rm min}^4) & \text{(anapole)}\,, \\ g_\chi^2 g_e^2\langle s^2\rangle\log(q_{\rm max}/q_{\rm min}) & \text{(pseudo-mediated)}\,. \end{cases} \qquad (13)
\end{aligned}
$$

Here $\theta$ is the angle between $\boldsymbol{q}$ and $\boldsymbol{v}_\chi$, $\langle c^2\rangle$ and $\langle s^2\rangle$ are properly averaged values of cosine and sine squared of the angle between $\boldsymbol{q}$ and the ground state spin direction over accessible scattering kinematics, $q_{\rm max} \simeq 2m_\chi v_\chi$, and $q_{\rm min}$ is the magnon momentum for which $\omega_{\boldsymbol{q}} = \omega_{\rm min}$. The $q$ dependence in Eq. (13) is indicative of dipole-dipole, quadrupole-dipole and charge-dipole type interactions, respectively, for the three DM models.

The projected reach for this $n = 1$ Heisenberg ferromagnet is shown by the dashed curves in Fig. 1 in the $\omega_{\rm min} = 1\,\text{meV}$ case, with $\langle c^2\rangle$ set to 1/3. We see that the full YIG results are almost exactly reproduced in the intermediate mass regime $0.02\,\text{MeV} \lesssim m_\chi \lesssim 0.1\,\text{MeV}$. For the lowest $m_\chi$ shown, the gapless branch becomes kinematically inaccessible, and the YIG reach is dominated by the gapped magnons. Also, for $m_\chi \gtrsim 0.1\,\text{MeV}$, YIG beats the $n = 1$ ferromagnet due to contributions from the gapped magnons, which are no longer suppressed as the typical momentum transfer approaches (and goes beyond) the boundaries of the 1BZ. For higher $\omega_{\rm min}$, we have found that the agreement in the intermediate mass regime is less exact, as the lowest-energy magnon modes on the gapless branch become inaccessible.

*Discussion* — While we have chosen three specific DM models for illustration, we note that there are other scenarios of DM with SD interactions that can be probed via magnon excitation. Examples include models with a spin-1 mediator coupling to the axial vector current $\bar{e}\gamma^\mu\gamma^5 e$ or coupling nonminimally to the electron. Generally, $\hat{\mathcal{O}}_\chi^\alpha$ is the mediator propagator multiplied by a function that is at least linear in $q$, so the rate is at least logarithmic, as in the pseudo-mediated model (see Eq. (13)). Given the strong astrophysical and cosmo-

logical constraints on light DM and mediator scenarios [22, 55, 56], magnon excitations are most relevant for probing subcomponents of DM with SD interactions, if they are not mediated by a dark photon.

Beyond scattering, a magnon signal can also arise from absorption of bosonic DM. A prime example is an axion $a$ that couples to the electron via $(\partial_\mu a)\,\bar{e}\gamma^\mu\gamma^5 e \to \nabla a \cdot \boldsymbol{S}_e$. However, Heisenberg-type materials with 3d electrons, such as YIG, have very limited sensitivity to DM absorption, because the kinematics is such that only gapped modes with $k \simeq 0$ can contribute, for which the matrix element is strongly suppressed as explained above. Here we identify three possible solutions, which we plan to pursue in detail in future work. First, we can look for materials where the magnetic atoms/ions have nondegenerate Landé $g$-factors, due to different orbital angular momentum admixtures in the effective spins. In this case, the magnetic atoms/ions within the same unit cell can respond differently in the $q \to 0$ limit, thus exciting gapped magnons. Second, anisotropies in the spin-spin interactions can lift the otherwise gapless Goldstone modes due to reduced rotation symmetry of the Hamiltonian. This enables those modes to match DM absorption kinematics, thus significantly enhancing the rate despite the remaining gapped modes suffering from the same suppression as before. Finally, the gapless modes can also be lifted by an external magnetic field. An advantage of this approach is that for DM absorption, the magnetic field can be tuned to scan the DM mass, as considered in Refs. [47–49] in the context of axion absorption.

*Conclusions* — Collective excitations in condensed matter systems offer a novel detection path for light DM, as a result of favorable kinematics. Given our ignorance of how the DM may interact with SM particles, it is important to explore different types of collective excitations in various materials in order to cover the broadest range of possibilities. In this *Letter*, we have proposed using magnon excitations to detect DM in the 10 keV-10 MeV mass range that couples to the electron spin. This complements previous proposals of detecting spin-independent DM interactions via phonon excitation. We have shown that, in scenarios where spin-independent DM interactions are suppressed, such as where the DM couples to a dark photon via a magnetic dipole or anapole, and where a strongly-interacting subcomponent of DM couples via a scalar mediator to the pseudoscalar current of the electron, currently unconstrained models can be probed via magnon excitation. We have considered a YIG target to demonstrate the DM detection concept and rate calculation. Concrete experimental designs will be studied in future work.

*Acknowledgments* — We thank Sinéad Griffin, David Hsieh, Matt Pyle and Mengxing Ye for useful discussions, and Sinéad Griffin, Katherine Inzani and Thomas Harrelson for collaboration on future work. T.T., Z.Z. and K.Z. are supported by the DoE under contract DE-AC02-05CH11231. T.T. and K.Z. are also supported by the Quantum Information Science Enabled Discovery (QuantISED) for High Energy Physics (KA2401032). Z.Z. is also supported by the NSF grant PHY-1638509. We thank the CERN theory group for hospitality where part of this work was completed. Z.Z. and K.Z. also thank the Aspen Center for Physics for hospitality during the completion of this work.

[1] E. D. Carlson, M. E. Machacek, and L. J. Hall, Astrophys. J. **398**, 43 (1992).
[2] C. Boehm and P. Fayet, Nucl. Phys. **B683**, 219 (2004), arXiv:hep-ph/0305261 [hep-ph].
[3] M. J. Strassler and K. M. Zurek, Phys. Lett. **B651**, 374 (2007), arXiv:hep-ph/0604261 [hep-ph].
[4] M. Pospelov, A. Ritz, and M. B. Voloshin, Phys. Lett. **B662**, 53 (2008), arXiv:0711.4866 [hep-ph].
[5] D. Hooper and K. M. Zurek, Phys. Rev. **D77**, 087302 (2008), arXiv:0801.3686 [hep-ph].
[6] J. L. Feng and J. Kumar, Phys. Rev. Lett. **101**, 231301 (2008), arXiv:0803.4196 [hep-ph].
[7] T. Lin, H.-B. Yu, and K. M. Zurek, Phys. Rev. **D85**, 063503 (2012), arXiv:1111.0293 [hep-ph].
[8] Y. Hochberg, E. Kuflik, T. Volansky, and J. G. Wacker, Phys. Rev. Lett. **113**, 171301 (2014), arXiv:1402.5143 [hep-ph].
[9] R. Essig, J. Mardon, and T. Volansky, Phys. Rev. **D85**, 076007 (2012), arXiv:1108.5383 [hep-ph].
[10] P. W. Graham, D. E. Kaplan, S. Rajendran, and M. T. Walters, Phys. Dark Univ. **1**, 32 (2012), arXiv:1203.2531 [hep-ph].
[11] R. Essig, A. Manalaysay, J. Mardon, P. Sorensen, and T. Volansky, Phys. Rev. Lett. **109**, 021301 (2012), arXiv:1206.2644 [astro-ph.CO].
[12] S. K. Lee, M. Lisanti, S. Mishra-Sharma, and B. R. Safdi, Phys. Rev. **D92**, 083517 (2015), arXiv:1508.07361 [hep-ph].
[13] R. Essig, M. Fernandez-Serra, J. Mardon, A. Soto, T. Volansky, and T.-T. Yu, JHEP **05**, 046 (2016), arXiv:1509.01598 [hep-ph].
[14] S. Derenzo, R. Essig, A. Massari, A. Soto, and T.-T. Yu, Phys. Rev. **D96**, 016026 (2017), arXiv:1607.01009 [hep-ph].
[15] Y. Hochberg, T. Lin, and K. M. Zurek, Phys. Rev. **D95**, 023013 (2017), arXiv:1608.01994 [hep-ph].
[16] I. M. Bloch, R. Essig, K. Tobioka, T. Volansky, and T.-T. Yu, JHEP **06**, 087 (2017), arXiv:1608.02123 [hep-ph].
[17] R. Essig, T. Volansky, and T.-T. Yu, Phys. Rev. **D96**, 043017 (2017), arXiv:1703.00910 [hep-ph].
[18] N. A. Kurinsky, T. C. Yu, Y. Hochberg, and B. Cabrera, (2019), arXiv:1901.07569 [hep-ex].
[19] R. Essig, J. Mardon, O. Slone, and T. Volansky, Phys. Rev. **D95**, 056011 (2017), arXiv:1608.02940 [hep-ph].
[20] A. Arvanitaki, S. Dimopoulos, and K. Van Tilburg, Phys. Rev. **X8**, 041001 (2018), arXiv:1709.05354 [hep-ph].
[21] Y. Hochberg, Y. Zhao, and K. M. Zurek, Phys. Rev. Lett. **116**, 011301 (2016), arXiv:1504.07237 [hep-ph].

[22] Y. Hochberg, M. Pyle, Y. Zhao, and K. M. Zurek, JHEP **08**, 057 (2016), arXiv:1512.04533 [hep-ph].
[23] Y. Hochberg, T. Lin, and K. M. Zurek, Phys. Rev. **D94**, 015019 (2016), arXiv:1604.06800 [hep-ph].
[24] Y. Hochberg, Y. Kahn, M. Lisanti, C. G. Tully, and K. M. Zurek, Phys. Lett. **B772**, 239 (2017), arXiv:1606.08849 [hep-ph].
[25] K. Schutz and K. M. Zurek, Phys. Rev. Lett. **117**, 121302 (2016), arXiv:1604.08206 [hep-ph].
[26] S. Knapen, T. Lin, and K. M. Zurek, Phys. Rev. **D95**, 056019 (2017), arXiv:1611.06228 [hep-ph].
[27] S. Knapen, T. Lin, M. Pyle, and K. M. Zurek, (2017), arXiv:1712.06598 [hep-ph].
[28] S. Griffin, S. Knapen, T. Lin, and K. M. Zurek, Phys. Rev. **D98**, 115034 (2018), arXiv:1807.10291 [hep-ph].
[29] S. Chang, A. Pierce, and N. Weiner, JCAP **1001**, 006 (2010), arXiv:0908.3192 [hep-ph].
[30] A. L. Fitzpatrick and K. M. Zurek, Phys. Rev. **D82**, 075004 (2010), arXiv:1007.5325 [hep-ph].
[31] A. L. Fitzpatrick, W. Haxton, E. Katz, N. Lubbers, and Y. Xu, (2012), 10.1088/1475-7516/2013/02/004, arXiv:1203.3542.
[32] M. I. Gresham and K. M. Zurek, (2014), 10.1103/PhysRevD.89.123521, arXiv:1401.3739.
[33] M. Pospelov and T. ter Veldhuis, Phys. Lett. **B480**, 181 (2000), arXiv:hep-ph/0003010 [hep-ph].
[34] K. Sigurdson, M. Doran, A. Kurylov, R. R. Caldwell, and M. Kamionkowski, Phys. Rev. **D70**, 083501 (2004), [Erratum: Phys. Rev.D73,089903(2006)], arXiv:astro-ph/0406355 [astro-ph].
[35] E. Masso, S. Mohanty, and S. Rao, Phys. Rev. **D80**, 036009 (2009), arXiv:0906.1979 [hep-ph].
[36] S. Chang, N. Weiner, and I. Yavin, Phys. Rev. **D82**, 125011 (2010), arXiv:1007.4200 [hep-ph].
[37] V. Barger, W.-Y. Keung, and D. Marfatia, Phys. Lett. **B696**, 74 (2011), arXiv:1007.4345 [hep-ph].
[38] T. Banks, J.-F. Fortin, and S. Thomas, (2010), arXiv:1007.5515 [hep-ph].
[39] C. M. Ho and R. J. Scherrer, Phys. Lett. **B722**, 341 (2013), arXiv:1211.0503 [hep-ph].
[40] E. Del Nobile, G. B. Gelmini, P. Gondolo, and J.-H. Huh, JCAP **1406**, 002 (2014), arXiv:1401.4508 [hep-ph].
[41] B. J. Kavanagh, P. Panci, and R. Ziegler, JHEP **04**, 089 (2019), arXiv:1810.00033 [hep-ph].
[42] X. Chu, J. Pradler, and L. Semmelrock, Phys. Rev. **D99**, 015040 (2019), arXiv:1811.04095 [hep-ph].
[43] A. Auerbach, *Interacting electrons and quantum magnetism* (Springer, 1994).
[44] J. M. D. Coey, *Magnetism and magnetic materials* (Cambridge University Press, 2009).
[45] V. Cherepanov, I. Kolokolov, and V. L'vov, Physics Reports **229**, 81 (1993).
[46] A. J. Princep, R. A. Ewings, S. Ward, S. Tóth, C. Dubs, D. Prabhakaran, and A. T. Boothroyd, npj Quantum Materials **2**, 63 (2017).
[47] R. Barbieri, M. Cerdonio, G. Fiorentini, and S. Vitale, Phys. Lett. **B226**, 357 (1989).
[48] N. Crescini *et al.*, Eur. Phys. J. **C78**, 703 (2018), [Erratum: Eur. Phys. J.C78,no.9,813(2018)], arXiv:1806.00310 [hep-ex].
[49] G. Flower, J. Bourhill, M. Goryachev, and M. E. Tobar, Phys. Dark Univ. , 100306 (2018), arXiv:1811.09348 [physics.ins-det].
[50] A. Jain, S. P. Ong, G. Hautier, W. Chen, W. D. Richards, S. Dacek, S. Cholia, D. Gunter, D. Skinner, G. Ceder, and K. a. Persson, APL Materials **1**, 011002 (2013).
[51] S. Toth and B. Lake, (2014), 10.1088/0953-8984/27/16/166002, arXiv:1402.6069.
[52] R. Essig, M. Sholapurkar, and T.-T. Yu, Phys. Rev. **D97**, 095029 (2018), arXiv:1801.10159 [hep-ph].
[53] S. Davidson, S. Hannestad, and G. Raffelt, JHEP **05**, 003 (2000), arXiv:hep-ph/0001179 [hep-ph].
[54] H. Vogel and J. Redondo, JCAP **1402**, 029 (2014), arXiv:1311.2600 [hep-ph].
[55] D. Green and S. Rajendran, JHEP **10**, 013 (2017), arXiv:1701.08750 [hep-ph].
[56] S. Knapen, T. Lin, and K. M. Zurek, Phys. Rev. **D96**, 115021 (2017), arXiv:1709.07882 [hep-ph].
[57] Y. Hinuma, G. Pizzi, Y. Kumagai, F. Oba, and I. Tanaka, arXiv:1602.06402.


## APPENDIX: ADDITIONAL DETAILS OF THE MAGNON RATE CALCULATION

Here we provide additional technical details of the calculations in the *Letter*. We begin by reviewing the derivation of the magnon Hamiltonian Eq. (3). We first define a local coordinate system for each sublattice $j$, in which the spins point in the $z$ direction in the ground state. Denoting the rotation matrices between global and local coordinates by $R_j$, we have

$$S^\alpha_{lj} = \sum_\beta R^{\alpha\beta}_j S'^\beta_{lj}\,, \quad \{\langle S'^1_{lj}\rangle, \langle S'^2_{lj}\rangle, \langle S'^3_{lj}\rangle\} = \{0,\, 0,\, S_j\}\,, \tag{A.1}$$

where $\alpha$, $\beta$ are Cartesian coordinates. To find the excitations above the ground state, we map the spin system onto a bosonic system via the Holstein-Primakoff transformation,

$$S'^+_{lj} = \left(2S_j - \hat{a}^\dagger_{lj}\hat{a}_{lj}\right)^{1/2}\hat{a}_{lj}\,, \qquad S'^-_{lj} = \hat{a}^\dagger_{lj}\left(2S_j - \hat{a}^\dagger_{lj}\hat{a}_{lj}\right)^{1/2}, \qquad S'^3_{lj} = S_j - \hat{a}^\dagger_{lj}\hat{a}_{lj}\,, \tag{A.2}$$

where $S'^\pm_{lj} = S'^1_{lj} \pm iS'^2_{lj}$. The bosonic creation and annihilation operators satisfy $[\hat{a}_{lj}, \hat{a}^\dagger_{l'j'}] = \delta_{ll'}\delta_{jj'}$, so that commutators between the spin operators $[S'^\alpha_{lj}, S'^\beta_{l'j'}] = \delta_{ll'}\delta_{jj'}\, i\epsilon^{\alpha\beta\gamma}S'^\gamma_{lj}$ are reproduced. Going to momentum space and

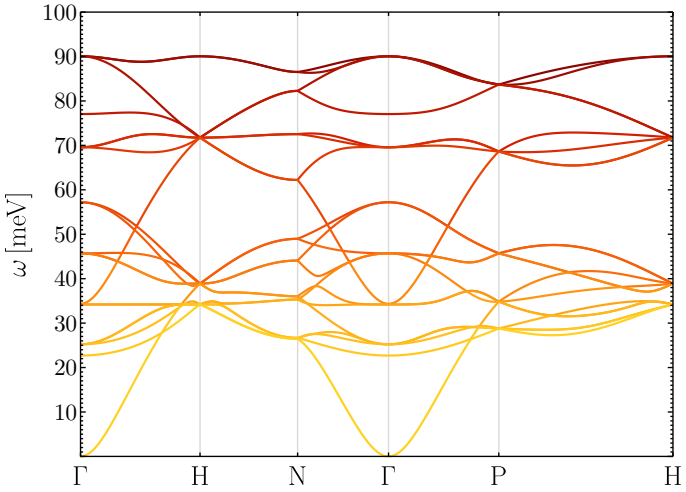


FIG. 2. Calculated magnon dispersion of YIG along the high symmetry lines in the first Brillouin zone.

diagonalizing the quadratic Hamiltonian (corresponding to the leading terms in the $1/S$ expansion) by a Bogoliubov transformation,

$$\hat{a}_{lj} = \frac{1}{\sqrt{N}} \sum_{\boldsymbol{k}\in 1\mathrm{BZ}} \hat{a}_{j,\boldsymbol{k}} e^{i\boldsymbol{k}\cdot\boldsymbol{x}_{lj}} \,, \tag{A.3}$$

$$\begin{pmatrix} \hat{a}_{j,\boldsymbol{k}} \\ \hat{a}^\dagger_{j,-\boldsymbol{k}} \end{pmatrix} = \mathrm{T}_{\boldsymbol{k}} \begin{pmatrix} \hat{b}_{\nu,\boldsymbol{k}} \\ \hat{b}^\dagger_{\nu,-\boldsymbol{k}} \end{pmatrix} \qquad \text{where} \quad \mathrm{T}_{\boldsymbol{k}} = \begin{pmatrix} \mathrm{U}_{j\nu,\boldsymbol{k}} & \mathrm{V}_{j\nu,\boldsymbol{k}} \\ \mathrm{V}^*_{j\nu,-\boldsymbol{k}} & \mathrm{U}^*_{j\nu,-\boldsymbol{k}} \end{pmatrix}, \tag{A.4}$$

where $\boldsymbol{x}_{lj}$ is the position of the $j$th site in the $l$th unit cell, we arrive at the free magnon Hamiltonian Eq. (3),

$$H = \sum_{\nu=1}^{n} \sum_{\boldsymbol{k}\in 1\mathrm{BZ}} \omega_{\nu,\boldsymbol{k}} \hat{b}^\dagger_{\nu,\boldsymbol{k}} \hat{b}_{\nu,\boldsymbol{k}} \,, \tag{A.5}$$

where $b^\dagger_{\nu,\boldsymbol{k}}, \hat{b}_{\nu,\boldsymbol{k}}$ are creation and annihilation operators for the canonical magnon modes. The canonical commutators are preserved, $[\hat{b}_{\nu,\boldsymbol{k}}, \hat{b}^\dagger_{\nu',\boldsymbol{k}'}] = \delta_{\nu\nu'}\delta_{\boldsymbol{k}\boldsymbol{k}'}$, by imposing the following constraint,

$$\mathrm{T}_{\boldsymbol{k}} \begin{pmatrix} \mathbb{1}_n & \mathbb{0}_n \\ \mathbb{0}_n & -\mathbb{1}_n \end{pmatrix} \mathrm{T}^\dagger_{\boldsymbol{k}} = \begin{pmatrix} \mathbb{1}_n & \mathbb{0}_n \\ \mathbb{0}_n & -\mathbb{1}_n \end{pmatrix}. \tag{A.6}$$

We follow the algorithm in Ref. [51] to solve the constrained diagonalization problem to obtain $\omega_{\nu,\boldsymbol{k}}$, $\mathrm{T}_{\boldsymbol{k}}$. Note that Ref. [51] uses a different Fourier transformation convention, with $\boldsymbol{x}_l$ rather than $\boldsymbol{x}_{lj}$ in the exponent of Eq. (A.3). We have consistently followed our convention throughout the calculation, adjusting the equations in Ref. [51] where necessary. In Fig. 2, we plot our calculated magnon dispersion $\omega_{\nu,\boldsymbol{k}}$ for YIG along the high symmetry lines in the (body-centered cubic) 1BZ generated using the SeeK-path code [57].

Next, we derive the single magnon production matrix element Eq. (5) from the DM-electron spin coupling Eq. (4). Assuming the absence of orbital angular momentum, a magnetic atom/ion at site $l, j$ sources an effective scattering potential for the incoming DM, which is given by the Fourier transform of the momentum space operator,

$$V_{lj}(\boldsymbol{x}) = \int \frac{d^3q}{(2\pi)^3} \sum_\alpha \hat{\mathcal{O}}^\alpha_\chi(\boldsymbol{q}) \hat{S}^\alpha_{lj}\, e^{-i\boldsymbol{q}\cdot(\boldsymbol{x}-\boldsymbol{x}_{lj})} \,. \tag{A.7}$$

For a DM particle with incoming momentum $\boldsymbol{p}$ and outgoing momentum $\boldsymbol{p}' = \boldsymbol{p} - \boldsymbol{q}$, and a transition $\lambda_i \to \lambda_f$ in the target system, the matrix element is

$$\mathcal{M} = \langle \chi_f \lambda_f | \hat{V} | \chi_i \lambda_i \rangle = \frac{1}{N\Omega} \sum_{lj} \int d^3x\, e^{i\boldsymbol{q}\cdot\boldsymbol{x}} \langle s_f \lambda_f | V_{lj}(\boldsymbol{x}) | s_i \lambda_i \rangle = \frac{1}{N\Omega} \sum_\alpha \langle s_f | \hat{\mathcal{O}}^\alpha_\chi(\boldsymbol{q}) | s_i \rangle \sum_{lj} e^{i\boldsymbol{q}\cdot\boldsymbol{x}_{lj}} \langle \lambda_f | \hat{S}^\alpha_{lj} | \lambda_i \rangle \,. \tag{A.8}$$

Now focus on the case where $\lambda_i$ is the ground state $|0\rangle$ and $\lambda_f$ is a single magnon state $|\nu, \boldsymbol{k}\rangle$. Plugging in Eqs. (A.1)-(A.4), and keeping only terms proportional to a single power of $\hat{b}^\dagger_{\nu,\boldsymbol{k}}$, we obtain

$$\begin{aligned}
\sum_{lj} e^{i\boldsymbol{q}\cdot\boldsymbol{x}_{lj}} \langle\lambda_f|\hat{S}^\alpha_{lj}|\lambda_i\rangle &= \sum_{lj} e^{i\boldsymbol{q}\cdot\boldsymbol{x}_{lj}} \sum_\beta \langle\nu,\boldsymbol{k}|R^{\alpha\beta}_j \hat{S}'^\beta_{lj}|0\rangle = \sum_{lj} \sqrt{\frac{S_j}{2}} e^{i\boldsymbol{q}\cdot\boldsymbol{x}_{lj}} \langle\nu,\boldsymbol{k}|r^{\alpha*}_j \hat{a}_{lj} + r^\alpha_j \hat{a}^\dagger_{lj}|0\rangle \\
&= \frac{1}{\sqrt{N}} \sum_{\boldsymbol{k}'\in 1\mathrm{BZ}} \sum_l e^{i(\boldsymbol{q}-\boldsymbol{k}')\cdot\boldsymbol{x}_l} \sum_j \sqrt{\frac{S_j}{2}}\, e^{i(\boldsymbol{q}-\boldsymbol{k}')\cdot\boldsymbol{x}_j} \langle\nu,\boldsymbol{k}|r^{\alpha*}_j \hat{a}_{j,-\boldsymbol{k}'} + r^\alpha_j \hat{a}^\dagger_{j,\boldsymbol{k}'}|0\rangle \\
&= \sqrt{N} \sum_{\boldsymbol{k}'\in 1\mathrm{BZ}} \sum_{\boldsymbol{G}} \delta_{\boldsymbol{q}-\boldsymbol{k}',\boldsymbol{G}} \sum_{j\nu'} \sqrt{\frac{S_j}{2}}\, e^{i\boldsymbol{G}\cdot\boldsymbol{x}_j} \left(\mathrm{V}_{j\nu',-\boldsymbol{k}'} r^{\alpha*}_j + \mathrm{U}^*_{j\nu',\boldsymbol{k}'} r^\alpha_j\right) \langle\nu,\boldsymbol{k}|\hat{b}^\dagger_{\nu',\boldsymbol{k}'}|0\rangle \\
&= \sqrt{N} \sum_{\boldsymbol{G}} \delta_{\boldsymbol{q}-\boldsymbol{k},\boldsymbol{G}} \sum_j \sqrt{\frac{S_j}{2}}\, e^{i\boldsymbol{G}\cdot\boldsymbol{x}_j} \left(\mathrm{V}_{j\nu,-\boldsymbol{k}} r^{\alpha*}_j + \mathrm{U}^*_{j\nu,\boldsymbol{k}} r^\alpha_j\right), \qquad \text{(A.9)}
\end{aligned}$$

where we have used $\boldsymbol{x}_{lj} = \boldsymbol{x}_l + \boldsymbol{x}_j$, $\sum_l e^{i(\boldsymbol{q}-\boldsymbol{k}')\cdot\boldsymbol{x}_l} = N \sum_{\boldsymbol{G}} \delta_{\boldsymbol{q}-\boldsymbol{k}',\boldsymbol{G}}$. Plugging Eq. (A.9) into Eq. (A.8) reproduces Eq. (5) (where the sum over $\boldsymbol{G}$ is implicit).

Finally, we derive the analytical approximation for the rate in the case of an $n = 1$ ferromagnet target, Eqs. (12) and (13). Noting that the $\boldsymbol{k}$ integral over the 1BZ combined with the $\boldsymbol{G}$ sum is equivalent to an integral over the entire momentum space, we have

$$R = \frac{n_s}{\rho_T} \frac{\rho_\chi}{m_\chi} \int d^3 v_\chi\, f(\boldsymbol{v}_\chi) \int \frac{d^3 q}{8\pi^2}\, \mathrm{tr}\big(\hat{\rho}_\chi \hat{\mathcal{O}}^+_\chi(\boldsymbol{q}) \hat{\mathcal{O}}^{\dagger -}_\chi(\boldsymbol{q})\big)\, \delta\Big(\boldsymbol{q}\cdot\boldsymbol{v}_\chi - \frac{q^2}{2m_\chi} - \omega_{\boldsymbol{k}=\boldsymbol{q}-\boldsymbol{G}}\Big). \qquad \text{(A.10)}$$

Since the magnon dispersion is near isotropic, the delta function fixes the angle between $\boldsymbol{q}$ and $\boldsymbol{v}_\chi$ for any given $q = |\boldsymbol{q}|$ — this is true as long as $\frac{q^2}{2m_\chi} + \omega \leq q v_\chi$, or approximately (since $\omega \ll q v_\chi$), $q \leq 2 m_\chi v_\chi$. Thus,

$$R = \frac{n_s}{\rho_T} \frac{\rho_\chi}{m_\chi} \int d^3 v_\chi\, \frac{f(\boldsymbol{v}_\chi)}{v_\chi} \int_\Sigma \frac{dq\, d\phi}{8\pi^2}\, q\, \mathrm{tr}\big(\hat{\rho}_\chi \hat{\mathcal{O}}^+_\chi(\boldsymbol{q}) \hat{\mathcal{O}}^{\dagger -}_\chi(\boldsymbol{q})\big), \qquad \text{(A.11)}$$

where the $q$ integral is now over a two-dimensional surface $\Sigma$ that satisfies the energy-conserving delta function, which is approximately a sphere of radius $m_\chi v_\chi$ centered at $m_\chi \boldsymbol{v}_\chi$. The trace generally depends on the angle $\theta_q$ between $\boldsymbol{q}$ and the spins. For the three models in Table I, we have

$$\mathrm{tr}\big(\hat{\rho}_\chi \hat{\mathcal{O}}^+_\chi \hat{\mathcal{O}}^{\dagger -}_\chi\big) = \begin{cases} \frac{4 g_\chi^2 g_e^2}{\Lambda^2 m_e^2} \left(1 + \cos^2\theta_q\right) & \text{(magnetic dipole DM)}\,, \\ \frac{g_\chi^2 g_e^2}{\Lambda^4 m_e^2}\, q^2 \left(1 + \cos^2\theta_q\right) & \text{(anapole DM)}\,, \\ \frac{y_\chi^2 y_e^2}{m_e^2}\, \frac{1}{q^2}\, \sin^2\theta_q & \text{(pseudo-mediated DM)}\,. \end{cases} \qquad \text{(A.12)}$$

However, since the trigonometric functions are bounded, we have, *e.g.*, $\int dq d\phi\, f(q) \cos^2\theta_q = 2\pi \langle c^2\rangle \int dq\, f(q)$ for a general function $f(q)$, with $\langle c^2\rangle \in [0, 1]$ a constant to be understood as a weighted average of $\cos^2\theta_q$ over the integration region. Thus,

$$R = \frac{n_s}{\rho_T} \frac{\rho_\chi}{m_\chi} \int d^3 v_\chi\, \frac{f(\boldsymbol{v}_\chi)}{v_\chi} \int_{q_{\min}(\omega_{\min})}^{q_{\max}(v_\chi)} \frac{dq}{4\pi}\, q \left\langle \mathrm{tr}\big(\hat{\rho}_\chi \hat{\mathcal{O}}^+_\chi(\boldsymbol{q}) \hat{\mathcal{O}}^{\dagger -}_\chi(\boldsymbol{q})\big)\right\rangle. \qquad \text{(A.13)}$$

After performing the $q$ integral, we arrive at Eqs. (12) and (13).